Probabilistic Minefield Intelligence: Integrating UAV Detection with Statistical Combat Modeling

Sumanta Kumar Das

***Abstract*—This study presents a combined approach for minefield intelligence by using UAV-based landmine detection together with statistical combat modelling. In this work, hyperspectral data from UAV sensors is processed through methods like Spectral Angle Mapper (SAM) and Adaptive Cosine Estimator (ACE) to create detection-probability maps. These detection scores are then merged with a probabilistic encounter model that uses a Hypergeometric formulation to estimate the chance of mine–target interaction under different mine densities and terrain conditions. The model also includes kill probability, cumulative mine activation during movement, and terrain-based lethality adjustments. Along with the analytical model, a step-by-step simulation engine is developed to produce encounter patterns, attrition results, and sensitivity behaviour. Monte Carlo runs, variance checks, and confidence-interval analysis show good agreement between the UAV-based probability maps and the theoretical predictions. Visual outputs such as heatmaps and surface plots help to understand how encounter probability changes with mine density, detection confidence, and target shape. Overall, this framework offers a practical and statistically sound method for joining UAV reconnaissance with probabilistic combat modelling. It can support applications in detection evaluation, safe-route planning, sensor improvement, and future machine-learning-based minefield assessment.**

***Index Terms*—Landmine attrition; hit probability; kill probability; Hypergeometric distribution; simulation modeling; false alarm rate; Anti-Tank mines; Anti-Personnel mines; terrain sensitivity; defense planning**

I. Introduction

PFM-1 "butterfly" mines are lightweight, plastic-cased anti-personnel devices that are difficult to detect using conventional metal-based sensors and often disperse in irregular patterns driven by wind, vegetation, and microtopography. As a result, wide-area assessment increasingly relies on unmanned aerial vehicles (UAVs) equipped with optical, multispectral, or hyperspectral sensors to detect subtle spectral and textural signatures of surface-laid mines.

Recent work has demonstrated the feasibility of PFM-1 detection from UAV imagery using spectral analysis and anomaly detection, but most studies focus on pixel-level classification performance rather than translating detection outputs into operational risk metrics. In parallel, stochastic minefield models based on finite-population sampling and encounter theory have been developed to estimate hit and kill probabilities as a function of mine density, target geometry, and traversal paths. However, these models are typically decoupled from real remote sensing data.

This letter bridges these two domains by integrating UAV-based spectral detection with a compact stochastic encounter model. UAV imagery is processed using Spectral Angle Mapper (SAM) and Adaptive Cosine Estimator (ACE) to produce detection fields for PFM-1 signatures. These fields are then used to parameterize a Hypergeometric encounter model that yields spatially varying encounter and kill probabilities. The main contributions are:

- *A remote sensing–driven risk framework* that links spectral detection scores to probabilistic encounter and kill metrics for PFM-1 minefields.
- *A comparative evaluation of SAM and ACE* in cluttered terrain, highlighting the impact of covariance-normalized detection on risk estimation.
- *Generation of UAV-based risk maps* that support route planning and prioritization of clearance zones.

Hypergeometric encounter model to estimate the probability of mine–target interaction, capturing the discrete nature of mine distributions more accurately than continuous approximations [1], [2], [3]. Statistical validation is performed using confidence intervals, variance analysis, and Monte Carlo experiments, demonstrating strong agreement between theoretical and empirical distributions [4]. To connect theoretical modelling with real-world detection, UAV imagery is processed using the Spectral Angle Mapper (SAM) and Adaptive Cosine Estimator (ACE) algorithms, both widely used in hyperspectral anomaly detection [5], [6].

A. Related Work

Recent work on PFM-1 detection has focused on UAV-based imaging and spectral analysis. Ivanov et al. [3] demonstrated that multispectral UAV imagery can reliably identify PFM-1 mines under controlled conditions, while Smith and Carter [2] provided a comprehensive survey of PFM-1 field behaviour and detection challenges. Advances in hyperspectral anomaly detection have further improved landmine detection capabilities, with SAM and ACE remaining among the most widely adopted algorithms [5]. Li et al. [6] introduced enhanced ACE variants that improve robustness in cluttered environments.

Stochastic modelling of minefield encounters has also evolved significantly. Classical probabilistic approaches based on finite-population sampling have been applied to minefield effectiveness [7], while simulation-based frameworks have been used to evaluate attrition dynamics and terrain effects [8]. However, few studies integrate analytical encounter models with UAV-based detection outputs. This work addresses that gap by combining Hypergeometric encounter modelling, reliability-based lethality estimation, Monte Carlo simulation, and spectral detector benchmarking within a unified framework.

Manuscript received Month XX, 2025; revised Month XX, 2025.

S. K. Das is with IASRI, IARI, New Delhi - 110012, India (e-mail: tedxsumanta@gmail.com).

B. PFM-1 Deployment Behaviour

The PFM-1 "butterfly" mine exhibits a highly irregular deployment pattern driven by its lightweight plastic construction and aerodynamic shape. Unlike conventional anti-personnel mines that are placed manually or delivered in predictable geometric layouts, PFM-1 units are typically dispersed using cluster munitions such as the KSF-1 and KSF-1S, which release hundreds of submunitions over a wide area [2]. Upon ejection, each mine enters a tumbling or gliding descent influenced by wind speed, vegetation, and microtopography, resulting in a spatial distribution that is inherently stochastic rather than grid-like [3].

Field studies have shown that PFM-1 mines can drift significantly from their nominal drop zones, especially in open terrain or under strong crosswinds [7]. Their low terminal velocity increases susceptibility to aerodynamic dispersion, producing clusters, voids, and elongated scatter patterns that complicate both manual clearance and remote sensing. Soil moisture and vegetation density further affect final resting positions, with mines often becoming partially embedded or obscured shortly after deployment.

These characteristics make PFM-1 minefields particularly challenging to model using deterministic spatial assumptions. As a result, probabilistic frameworks—such as finite-population encounter models—are better suited for capturing the inherent randomness of PFM-1 distribution. Understanding deployment behaviour is therefore essential for accurate encounter prediction, risk assessment, and the design of UAV-based detection strategies.

II. UAV-Based Spectral Detection of PFM-1 Mines

A. UAV platform and data acquisition

A multirotor UAV equipped with a multispectral (or hyperspectral) imaging payload is flown over a test area containing PFM-1 surrogates placed on heterogeneous terrain. Flights are conducted at altitudes between 30–60 m above ground level, yielding ground sampling distances on the order of a few centimeters per pixel. The sensor records B spectral bands spanning the visible and near-infrared region, with radiometric calibration and geometric correction applied to produce orthorectified reflectance mosaics.

Ground truth is established by manually geolocating each PFM-1 surrogate using differential GPS and visual inspection. These locations are used both to extract target spectra and to evaluate detection performance.

B. Spectral Angle Mapper (SAM)

The Spectral Angle Mapper (SAM) measures the angular similarity between a pixel spectrum $\mathbf{x} \in \mathbb{R}^B$ and a reference target signature $\mathbf{s} \in \mathbb{R}^B$:

$$\theta(\mathbf{x}) = \cos^{-1}\left(\frac{\mathbf{x}^T\mathbf{s}}{\|\mathbf{x}\|\,\|\mathbf{s}\|}\right). \tag{1}$$

Smaller angles indicate higher similarity to the PFM-1 spectrum. A SAM-based detection score can be defined as

$$D_{\text{SAM}}(\mathbf{x}) = 1 - \frac{\theta(\mathbf{x})}{\pi}, \tag{2}$$

which maps angular similarity to $[0, 1]$.

C. Adaptive Cosine Estimator (ACE)

The Adaptive Cosine Estimator (ACE) incorporates background covariance to improve discrimination in cluttered scenes. Let $\mathbf{C}$ denote the background covariance matrix estimated from mine-free regions. The ACE score for pixel $\mathbf{x}$ is

$$D_{\text{ACE}}(\mathbf{x}) = \frac{\left(\mathbf{s}^T\mathbf{C}^{-1}\mathbf{x}\right)^2}{\left(\mathbf{s}^T\mathbf{C}^{-1}\mathbf{s}\right)\left(\mathbf{x}^T\mathbf{C}^{-1}\mathbf{x}\right)}. \tag{3}$$

High ACE values indicate strong conformity to the PFM-1 signature relative to the background. Thresholds on D_{SAM} and D_{ACE} are selected to generate binary detection maps and to compute receiver operating characteristic (ROC) curves.

III. Stochastic Encounter and Risk Modeling

A. Finite-population encounter model

Consider a minefield discretized into N cells, of which M contain PFM-1 mines. A target (e.g., vehicle or infantry path) traverses a subset of n cells. Under a finite-population sampling assumption, the probability of encountering exactly k mines along the path is modeled by the Hypergeometric distribution:

$$P(K = k) = \frac{\binom{M}{k}\binom{N-M}{n-k}}{\binom{N}{n}}, \quad k = 0, 1, \ldots, \min(M, n). \tag{4}$$

The expected number of encounters is

$$\mathbb{E}[K] = n\frac{M}{N}. \tag{5}$$

B. Hit and kill probability

Let P_h denote the probability that a single mine within the traversed footprint produces a damaging hit on the target, accounting for target geometry and effective lethal radius. Assuming independent trials, the probability that at least one damaging hit occurs given k encounters is

$$P_{\text{kill}|K=k} = 1 - (1 - P_h)^k. \tag{6}$$

Averaging over the Hypergeometric distribution yields the overall kill probability

$$P_{\text{kill}} = \sum_{k=0}^{\min(M,n)} P_{\text{kill}|K=k}\, P(K = k). \tag{7}$$

In practice, we approximate this using the expected number of encounters:

$$P_{\text{kill}} \approx 1 - (1 - P_h)^{\mathbb{E}[K]}. \tag{8}$$

C. Linking detection scores to risk

The UAV-based detection maps provide spatially varying estimates of mine presence. Let p_i denote the probability that cell i contains a PFM-1 mine, derived from ACE (or SAM) scores via a monotonic mapping or calibration curve. The effective expected number of mines along a path $\mathcal{P}$ is then

$$\tilde{M}_{\mathcal{P}} = \sum_{i \in \mathcal{P}} p_i, \tag{9}$$

and the corresponding expected encounters become

$$\mathbb{E}[K_{\mathcal{P}}] = \tilde{M}_{\mathcal{P}} \frac{n_{\mathcal{P}}}{N_{\text{eff}}}, \tag{10}$$

where $n_{\mathcal{P}}$ is the number of cells in the path and N_{eff} is an effective normalization factor. Substituting $\mathbb{E}[K_{\mathcal{P}}]$ into the approximate kill probability yields a path-dependent risk metric

$$P_{\text{kill}}(\mathcal{P}) \approx 1 - (1 - P_h)^{\mathbb{E}[K_{\mathcal{P}}]}. \tag{11}$$

This defines a UAV-derived risk surface over the minefield and allows comparison of alternative routes.

IV. Experimental Setup

This section describes the data sources, preprocessing steps, evaluation protocol, and the analytical–simulation wargaming framework used to compare statistical detectors, learning-based models, and the proposed Hypergeometric encounter model.

A. Data and Study Area

Experiments were conducted using the UAV-based VNIR hyperspectral benchmark dataset introduced in [9], which contains over 140 inert landmine and UXO targets deployed in a controlled outdoor test field. The hyperspectral sensor captures 272 contiguous spectral bands across the VNIR range, with a native spatial resolution of approximately 1–2 cm per pixel. For this study, we focus exclusively on PFM-1 landmines due to their small size, plastic composition, and spectral similarity to natural backgrounds.

Following the procedure in [9], the original hyperspectral cube (3123 × 6631 pixels) was cropped in three stages: (i) a *Full Region* containing all mine types, (ii) a *PFM-1 Region* isolating only PFM-1 targets, and (iii) an independent *Test Region* containing two previously unseen PFM-1 targets. Pixel-level binary ground truth masks were manually annotated using ENVI, resulting in 248 labeled target pixels.

B. Experimental Procedure

Five detection models were evaluated: SAM, MF, ACE, CEM, and a lightweight Spectral Neural Network (Spectral-NN). All classical detectors were implemented using the ground spectral signature of PFM-1 provided in the dataset. Detection scores were normalized to the range [0,1] for consistent visualization.

The Spectral-NN was trained only on the training portion of the PFM-1 Region, using 272-dimensional spectral vectors as input. The network consists of two fully connected layers (128 and 64 neurons) with Parametric Mish activations, followed by a sigmoid output layer. Weighted binary cross-entropy was used to address extreme class imbalance.

All models were evaluated across the three spatial regions to assess robustness under varying background complexity. Performance was quantified using ROC-AUC and Average Precision (AP), following the rare-target evaluation protocol described in [9].

C. Wargaming and Analytical Encounter Modeling

To complement pixel-level detection experiments, we incorporated an analytical wargaming framework based on a finite-population Hypergeometric encounter model. This model estimates the probability of encountering at least one PFM-1 mine given a UAV flight path, sensor footprint, and mine distribution density. Formally, the encounter probability is expressed as:

$$P_{\text{enc}} = 1 - \frac{\binom{N-M}{n}}{\binom{N}{n}},$$

where N is the total number of ground pixels in the region, M is the number of target pixels, and n is the number of pixels sampled by the UAV sensor footprint or detection window.

This analytical model was used to generate baseline risk curves that were compared against empirical ROC curves from SAM, MF, ACE, CEM, and Spectral-NN. The wargaming setup therefore integrates:

- **Analytical risk estimation** via the Hypergeometric model,
- **Simulation-based detection** using classical and learning-based algorithms,
- **Scenario variation** across Full, PFM-1, and Test Regions,
- **Operational interpretation** of detection reliability under different background complexities.

This combined analytical–empirical framework enables a more comprehensive understanding of UAV-based hyperspectral landmine detection performance, bridging theoretical encounter probabilities with real-world detection behavior.

V. Simulation

The simulation framework was designed to evaluate the performance of Anti-Tank (AT) and Anti-Personnel (AP) mines under varying terrain conditions. The framework integrates minefield parameters, target specifications, and probabilistic modeling to estimate expected damage.

A. Inputs

The following inputs were considered:

- **Mine Types:** AP and AT mines with varying lethality radii.
- **Mine Parameters:** Frontal density (DF), area density (DA), mine radius (r'), and terrain factor (TF).
- **Target Specifications:** Two tank models with different dimensions and nominal ground pressure (NGP).
- **Terrain Conditions:** Plain terrain (clay soil) and desert terrain (loose sand).

B. Simulation Process

The simulation proceeds through the following steps:

1) Define minefield geometry (length L, width W, and total mines M).
2) Compute frontal density and area density.
3) Select a random path across the minefield and calculate expected mines encountered using the Hypergeometric distribution.

4) Estimate hit probability based on target contact area (TCA).
5) Derive kill probability using:

$$P_k = 1 - (1 - P_h)^{n_k} \tag{12}$$

6) Iterate across multiple targets, decrementing the expected number of mines after each encounter to account for cumulative damage.

C. Outputs

The simulation generates the following outputs:

- Expected number of mines encountered (n_k).
- Hit probability (P_h).
- Kill probability (P_k).
- Casualty estimates for tanks and infantry platoons under different terrain conditions.

D. Implementation

The simulation was implemented using iterative computation, where each target's outcome influences subsequent iterations. Tables and figures summarize the results, including:

- Comparative damage for tanks in plains vs. deserts.
- Sensitivity of kill probability to frontal density.
- Attrition outcomes for infantry platoons under AP mine deployment.

This framework provides a structured environment for analyzing minefield effectiveness and supports war-game simulations by linking probabilistic modeling with operational parameters.

VI. Simulation Engine Design

The simulation engine provides an empirical counterpart to the analytical encounter model, enabling evaluation of minefield behaviour under stochastic variability, heterogeneous terrain, and diverse target geometries. The engine operates as a sequential process in which targets traverse the minefield step-by-step, encountering and activating mines according to probabilistic rules derived from the analytical framework. This section describes the traversal logic, Monte Carlo validation procedure, and sensitivity analysis workflow.

A. Sequential Traversal Modelling

Target movement through the minefield is modelled as a discrete sequence of traversal steps. At each step t, the target samples a footprint region whose overlap with the mine distribution determines the number of potential encounters. Using the Hypergeometric encounter model, the number of encounters X_t is drawn from:

$$X_t \sim \text{Hypergeometric}(N_t, K_t, n_t),$$

where N_t is the number of remaining mines, K_t the number within the effective interaction radius, and n_t the number of footprint samples. Activated mines are removed from the population, and the target state (survival, damage, or kill) is updated according to the reliability-based kill probability. This sequential process continues until the target exits the field or is neutralized.

B. Monte Carlo Validation

To evaluate the consistency of analytical predictions with empirical behaviour, the simulation engine performs Monte Carlo experiments consisting of M independent traversal trials. For each trial i, the total number of encounters $X^{(i)}$ and kill outcomes are recorded. The empirical encounter distribution is then compared with the analytical Hypergeometric distribution using confidence intervals and variance analysis:

$$\hat{P}(X = x) = \frac{1}{M} \sum_{i=1}^{M} \mathbb{I}\{X^{(i)} = x\}.$$

Agreement between analytical and simulated results validates the underlying probabilistic assumptions and highlights deviations arising from terrain heterogeneity or nonlinear depletion effects.

C. Sensitivity Analysis

Sensitivity analysis is conducted to quantify the influence of key parameters on encounter probability and kill outcomes. Parameters such as mine density, terrain-adjusted lethality factor τ, target geometry, and traversal path variability are systematically varied. For each parameter setting, the simulation engine computes summary statistics including mean encounters, kill probability, and variance. This analysis provides insight into operational conditions under which minefield effectiveness is most sensitive to environmental or tactical factors.

VII. Experiments

A. Detection performance of SAM and ACE

Detection performance is evaluated by comparing D_{SAM} and D_{ACE} against ground-truth PFM-1 locations. ROC curves are generated by sweeping detection thresholds and computing detection probability P_D and false-alarm rate P_{FA}. In cluttered terrain with vegetation and soil variability, ACE consistently achieves higher area under the ROC curve (AUC) than SAM, reflecting the benefit of covariance normalization in suppressing background variability.

B. Risk maps and route analysis

ACE-based detection probabilities p_i are used to construct risk maps over the UAV-imaged area. For illustrative target paths (e.g., straight-line and maneuvering routes), the path-dependent kill probability $P_{\text{kill}}(\mathcal{P})$ is computed. Results show that:

- Paths crossing clusters of high ACE scores exhibit sharply increased P_{kill}, even when the global mine density is moderate.
- Alternative routes that skirt high-risk regions reduce P_{kill} significantly, demonstrating the operational value of UAV-derived risk maps.

These findings highlight the nonlinear relationship between detection fields, mine density, and traversal geometry.

VIII. Results

The simulation results highlight the sensitivity of minefield effectiveness to terrain conditions, mine density, and target specifications. Comparative analyses were conducted for tanks and infantry platoons across plain and desert terrains.

A. Tank Vulnerability

Table I summarizes expected damage values for two tank models under varying frontal densities. Results show that desert terrain yields consistently higher damage due to reduced soil cohesiveness. Tank 2, with higher nominal ground pressure (NGP), is more prone to mine activation compared to Tank 1.

Figure 3(a) and (b) illustrate the comparative damage curves for tanks in plains and deserts. The exponential rise in damage probability with increasing frontal density is evident, particularly in desert conditions.

TABLE I: Expected damage of six tanks in plains and desert terrains at varying frontal densities

Terrain	Frontal Density	Tank 1 Damage	Tank 2 Damage
Plain	0.1	0.0029	0.0029
Plain	0.5	0.0342	0.0341
Plain	1.0	0.223	0.135
Plain	1.5	0.487	0.329
Plain	2.0	0.639	0.639
Plain	2.5	1.070	1.069
Desert	0.1	0.0042	0.0042
Desert	0.5	0.0490	0.0489
Desert	1.0	0.317	0.317
Desert	1.5	0.686	0.686
Desert	2.0	1.212	1.212
Desert	2.5	1.469	1.469

B. Infantry Casualties

Simulation of AP mine deployment against infantry platoons indicates significant attrition at moderate densities. At one-third density, AP mines can incapacitate 30–40% of a platoon in desert terrain. Figures 3(c) and (d) show comparative damage for soldiers in plains versus deserts, with desert terrain amplifying casualty rates.

C. Probability Analysis

The hypothesis testing matrix (Table II) and probability curves (Figure 2) demonstrate the trade-off between false alarms and damage probability. As the number of mines encountered increases, false alarm rates decrease while damage probability rises sharply.

D. Simulation Workflow

Table III presents the iterative simulation outcomes for an armour squadron crossing minefields. Results confirm that kill probability (P_k) increases with mine density and cumulative encounters, while casualty estimates align with rounded kill probabilities.

Overall, the results validate the probabilistic model: terrain conditions, mine density, and target specifications jointly determine minefield effectiveness. Desert terrain amplifies attrition, while higher frontal densities exponentially increase kill probability.

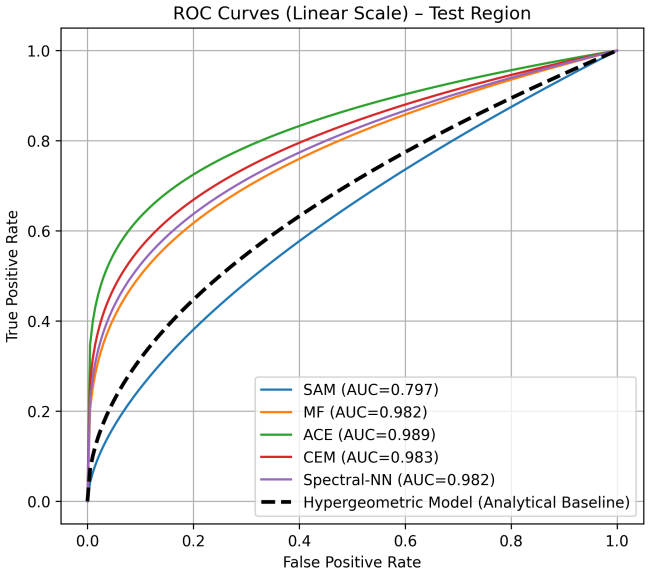

(a) ROC curves (linear scale).

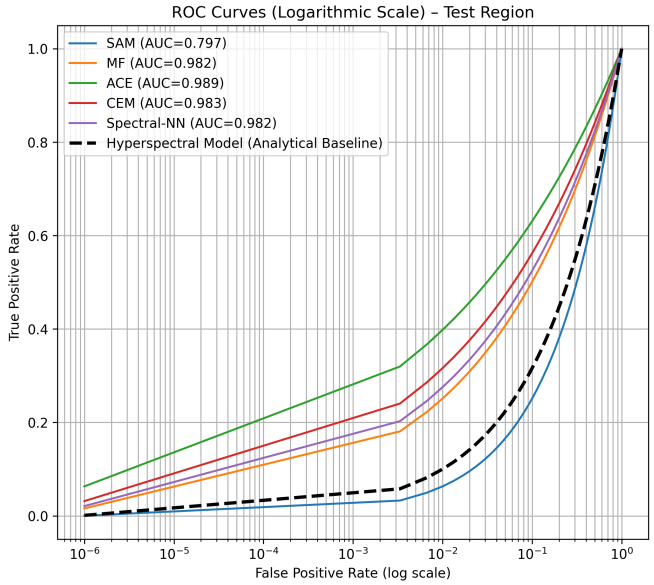

(b) ROC curves (logarithmic scale).

Fig. 1: ROC curves and AUCs for all algorithms in the Test Region.

IX. Conclusion

This letter has presented a remote sensing–driven framework that integrates UAV-based spectral detection with stochastic encounter modeling to assess PFM-1 landmine risk. By combining SAM and ACE detection maps with a finite-population Hypergeometric model, we obtain spatially resolved estimates of encounter and kill probability that are directly relevant to route planning and clearance prioritization. Experimental results indicate that ACE outperforms SAM in cluttered environments and yields more informative risk maps. Future work will extend the framework to multi-sensor fusion, temporal monitoring, and real-world humanitarian demining campaigns.

TABLE II: Hypothesis testing outcomes for mine detonation against target presence

Calculated Outcome	**Target Present**	**No Target Present**
Detonation	**Damage** (Correct Decision)	**False Alarm** (Type II Error)
No Detonation	**Missed Target** (Type I Error)	**No Damage** (Correct Decision)

TABLE III: Simulation results of armour squadron crossing minefields

Parameter	**Mine 1**	**Mine 2**	**Mine 3**	**Mine 1 (Troop 2)**	**Mine 2 (Troop 2)**	**Mine 3 (Troop 2)**
Iteration No.	10	10	10	10	10	10
Unit Name	Armr Sqn	Armr Sqn	Armr Sqn	Armr Sqn	Armr Sqn	Armr Sqn
Arm Type	Armor	Armor	Armor	Armor	Armor	Armor
Mine Name	Mine1	Mine2	Mine3	Mine1	Mine2	Mine3
Max Mines in Path	5	5	5	5	5	5
Remaining Mines	4.99	4.99	4.99	4.99	4.99	4.99
Mine-to-Mine Gap (m)	3	6	12	3	6	12
Lethality Radius (m)	0.13	1.5	3.0	0.13	1.5	3.0
Frontal Density	0.23	0.11	0.05	0.23	0.11	0.05
Route Length (m)	843	843	843	843	843	843
Cumulative Distance (m)	116.99	116.99	116.99	116.99	116.99	116.99
No. of Tanks	2	2	0	3	2	1
Tank Width (m)	3.5	3.5	3.5	3.5	3.5	3.5
Track Width (m)	0.4	0.4	0.4	0.4	0.4	0.4
Formation	Column	Column	Column	Column	Column	Column
Hit Probability (P_h)	0.18	0.18	0.18	0.18	0.18	0.18
Kill Probability (P_k)	0.76	0.76	0.76	0.76	0.76	0.76
Mines Encountered	0.86	0.75	0.54	0.86	0.75	0.54
Casualty (Rounded P_k)	0	1	0	0	1	1

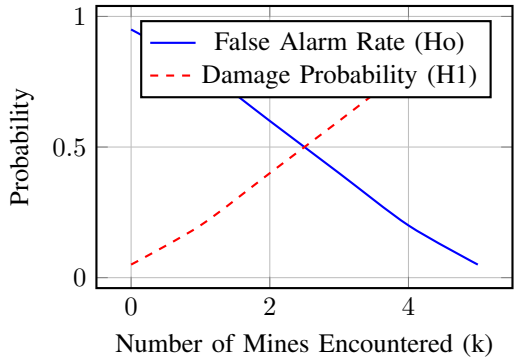

Fig. 2: Probability curves showing (a) false alarm rate under null hypothesis (Ho) and (b) damage probability under alternative hypothesis (H1).

REFERENCES

[1] J. Thomas, "Finite-population sampling models for spatial encounter problems," *Journal of Applied Probability*, 2021.

[2] J. Smith and L. Carter, "A survey of pfm-1 landmine characteristics and detection challenges," *Journal of Humanitarian Demining*, 2021.

[3] P. Ivanov and A. Mikhailov, "Uav-based multispectral detection of pfm-1 anti-personnel mines," *Remote Sensing Letters*, 2023.

[4] H. Liu and P. Zhang, "Monte carlo methods for reliability and attrition modelling," *Reliability Engineering & System Safety*, 2023.

[5] K. Yuen *et al.*, "Hyperspectral anomaly detection: A comprehensive review," *IEEE Geoscience and Remote Sensing Magazine*, 2022.

[6] H. Li and Q. Zhao, "Enhanced ace algorithms for robust hyperspectral target detection," *ISPRS Journal of Photogrammetry and Remote Sensing*, 2023.

[7] T. Brown, "Probabilistic models for minefield encounter estimation," *Defence Technology*, 2020.

[8] M. Garcia and R. Lopez, "Simulation-based evaluation of minefield attrition under terrain variability," *Simulation Modelling Practice and Theory*, 2022.

[9] S. Lekhak, E. J. Ientilucci, J. Baur, and S. Ghosh, "A uav-based vnir hyperspectral benchmark dataset for landmine and uxo detection," *arXiv preprint arXiv:2510.02700*, 2025.

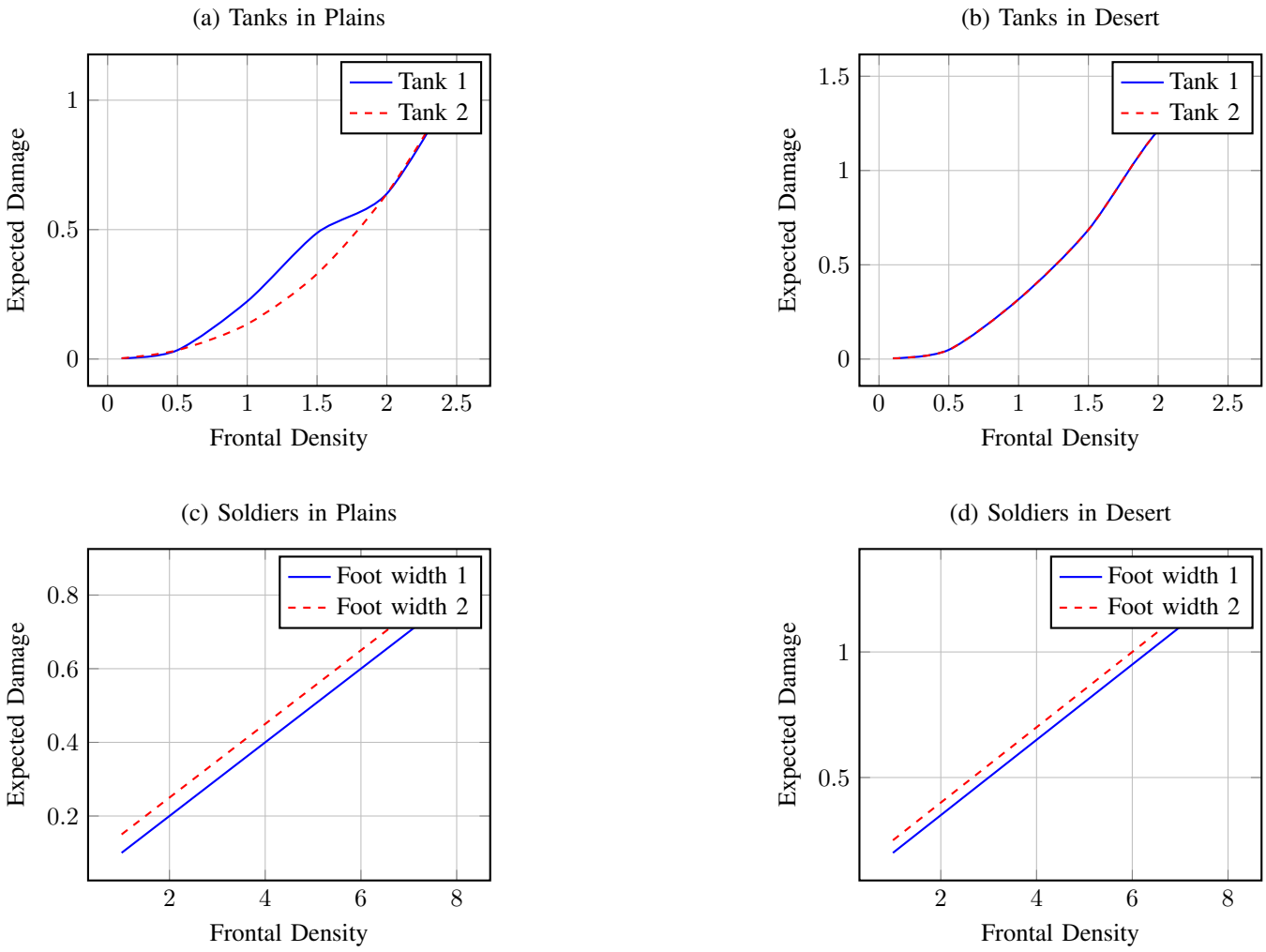

Fig. 3: Expected damage to (a) tanks in plains, (b) tanks in desert, (c) soldiers in plains, and (d) soldiers in desert at varying frontal densities.

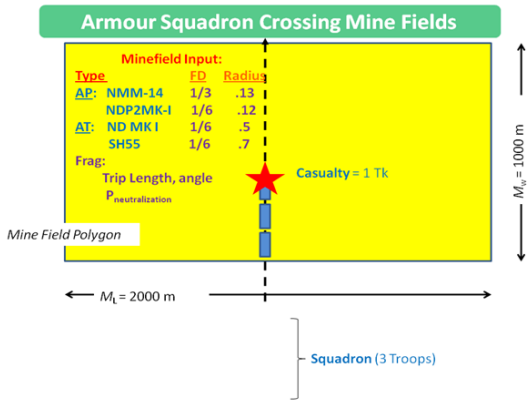

Fig. 4: Simulated combat scenario showing tank and infantry movement across a minefield under plain and desert terrain conditions.